MoS_2/Graphene Cocatalyst for Efficient Photocatalytic H_2 Evolution under Visible Light Irradiation

Kun Chang,[†] Zongwei Mei,[†] Tao Wang,[†] Qing Kang,[†] Shuxin Ouyang,[‡] and Jinhua Ye[†,‡,*]

[†]International Center for Materials Nanoarchitectonics (WPI-MANA), Environmental Remediation Materials Unit, 1-1 Namiki, Tsukuba, Ibaraki 305-0044, Japan and
[‡]TU-NIMS Joint Research Center, School of Material Science and Engineering, Tianjin University, 92 Weijin Road, Tianjin, P.R. China

ABSTRACT Exploiting noble-metal-free cocatalysts is of huge interest for photocatalytic water splitting using solar energy. Here we report a composite material consisting of CdS nanocrystals grown on the suface of a nanosized MoS_2/graphene hybrid as a high-performance noble-metal-free photocatalyst for H_2 evolution under visible light irradiation. Through the optimizing of each component proportion, the MoS_2/G-CdS composite showed the highest photocatalytic H_2 production activity when the content of the MoS_2/graphene cocatalyst is 2.0 wt % and the molar ratio of MoS_2 to graphene is 1:2. The photocatalytic H_2 evolution activity of the proposed MoS_2/G-CdS composite was tested and compared in Na_2S—Na_2SO_3 solution and lactic acid solution. A 1.8 mmol/h H_2 evolution rate in lactic acid solution corresponding to an AQE of 28.1% at 420 nm is not only higher than the case in Na_2S—Na_2SO_3 solution of 1.2 mmol/h but also much higher than that of Pt/CdS in lactic acid solution. The relative mechanism has been investigated. It is believed that this kind of MoS_2/G-CdS composite would have great potential as a promising photocatalyst with high efficiency and low cost for photocatalytic H_2 evolution reaction.

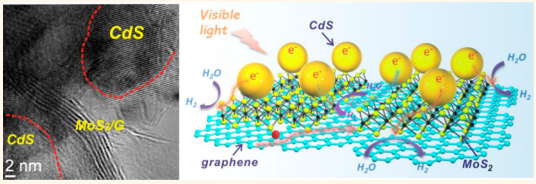

KEYWORDS: MoS_2/graphene-CdS · few-layer · photocatalyst · water splitting · visible light

The production of chemical fuels by using sunlight is an attractive and sustainable solution to global energy and environmental problems.[1] Since the 1970s, the discovery of a photoelectrochemical cell using TiO_2 supporting Pt electrodes for hydrogen evolution by Fujishima and Honda,[2] splitting water using solar energy has been a focus of great attention as a possible means for converting solar energy to chemical energy in the form of clean and renewable hydrogen fuel.[3] Up to now, a large number of semiconductor photocatalysts for hydrogen evolution have been developed.[4−9] However, most semiconductors cannot give high hydrogen evolution activities without a cocatalyst even in the presence of sacrificial agents, which is caused by the facile recombination of electron—hole pairs before migrating to the surface for reactions.[10,11] Generally, in order to retard the recombination of electron—hole pairs, metals, especially noble metals such as Pt, are always used to support the surface of semiconductors as cocatalysts.[12,13] The existence of cocatalysts not only effectively separates the electron—hole pairs but also provides more proton reductions sites, facilitating proton reduction reactions.

While the noble metals could be the efficient cocatalyts for semiconductors, due to their high cost, it is valuable to develop highly efficient and low-cost noble-metal-free cocatalysts to further facilitate the development of hydrogen evolution.[14,15] Recent studies indicate that some metal sulfides can be good candidates for cocatalysts.[16−18] As a typical layered transition metal sulfide, MoS_2, with a structure composed of three stacked atom layers (S—Mo—S) held together by van der Waals forces, has attracted much attention toward hydrogen evolution reactions (HERs).[19−21] Hinnemann *et al.* concluded through density functional calculations of free energy that the S atoms on exposed edges of MoS_2 have strong bonds to H^+ in the solution, which are easily reduced to H_2 by electrons.[22] Due to the active S atoms on exposed edges, which increases its activity for HER, MoS_2 is showing promise as a low-cost alternative to platinum. Recently, Kanda *et al.* reported that the MoS_2—TiO_2 system had good photocatalytic activity toward

* Address correspondence to Jinhua.YE@nims.go.jp.

Received for review April 10, 2014 and accepted June 9, 2014.

Published online June 13, 2014
10.1021/nn5019945

hydrogen generation.[23] Zhou *et al.* indicated that the TiO_2@MoS_2 heterostructure with 50 wt % MoS_2 exhibits the highest hydrogen production.[24] However, Zong *et al.* indicated that the junctions between MoS_2 and CdS could be more readily formed due to the common S^{2-} anions for each other, and MoS_2–CdS therefore exhibited high photocatalytic activities.[25] Theoretically, the cocatalytic activities of MoS_2 are caused only by the active S atoms on its exposed edges, but the S atoms on the basal plane have no activity. That is, nanosized MoS_2 with more exposed edges and active S atoms is supposed to deliver higher cocatalytic activities.

The poor electrical conductivity of MoS_2 restricts its cocatalytic activity; thus, photoelectrons can be derived from photocatalysts, and the recombination of electron–hole pairs is impeded. Recently, its electrical conductivity and activity for HER was improved through decreasing the MoS_2 layers and adding other conducting materials.[26−28] As a popular graphite-based material, graphene exhibits superior electron mobility and excellent electronic behavior.[29,30] In addition, graphene also has been reported to be an efficient cocatalyst for photocatalytic reactions because of its high specific surface area and good electron transfer abilities. Xiang *et al.* reported that MoS_2/graphene has higher cocatalytic activities on TiO_2 than pure MoS_2 and graphene.[31] They concluded that MoS_2/graphene as a cocatalyst can efficiently suppress charge recombination, improve interfacial charge transfer, and enhance photocatalytic activities. Thereby, it is expected that higher photocatalytic activities for noble-metal-free catalysts are achieved when MoS_2/graphene cocatalyst was supported on junction-matched CdS. Moreover, this kind of system can be achieved under visible light, further improving the efficiency of solar energy.

Herein, we report the fabrication of a nanosized layer-structured MoS_2/graphene nanosheet loaded with CdS nanoparticles with 3D hierarchical configuration by a solution-chemistry method and investigate its hydrogen production activities under visible light by optimizing each component's content in the MoS_2/graphene-CdS composite. This kind of structural catalyst not only can provide abundant reactive sites for hydrogen evolution but also can increase the transport of charges and reduce the recombination probability of photoexcited charge carriers. While in Na_2S–Na_2SO_3 solution the MoS_2/graphene-CdS composite shows lower hydrogen generation activities than Pt/CdS, and it showed much higher hydrogen generation activities than Pt/CdS in lactic acid solution, for which the reason was discussed. We believe that it should provide a choice of sacrificial agent for MoS_2-based photocatalysts toward hydrogen evolution reaction.

RESULTS AND DISCUSSION

Characterization of Morphology and Structure. The typical synthesis of the MoS_2/G-CdS composite is shown schematically in Figure 1a. First, microsized graphene oxide sheets could be cut into nanosized sheets by a hydrothermal reaction.[32,33] As shown in Figure 1b and c, after hydrothermal cutting, the reduced graphene oxide (RGO) nanosheets with a diameter of 200–300 nm are much smaller than that of as-prepared graphene oxide. Then as in our previous report,[34] MoS_2 nanosheets could be *in situ* grown on the surface of graphene, and decomposed sulfur nanoparticles from a portion of L-cysteine first anchored on the surface of graphene through nucleation, resulting in the formation and growth of MoS_2 nanosheets. A general view of MoS_2/G composite nanosheets is shown in Figure 1d and e. It can be seen that MoS_2/G composites consist of ultrathin 2D nanosheets with a diameter of 50–100 nm. Such nanosized 2D sheets are supposed to have more active exposed edges for HER. The high-resolution transmission electron microscopy (HRTEM) image (inset in Figure 1e) shows that MoS_2 layers with many defect sites and disordered structures are grown on the surface of reduced graphene oxide. This is because of the low synthesis temperature, which leads to the low crystallinity of MoS_2, and the X-ray diffraction (XRD) analysis in Figure 2c also indicates it is an amorphous MoS_2/G composite. Because of the large amount of defect sites and vacancies and the large surface area, Cd^{2+} ions are easily adsorbed on the MoS_2/G. Under the adhesive effect of polyvinylpyrrolidone (PVP), 3D hierarchical MoS_2/G-CdS composites with diameters of 100 to 300 nm are obtained (as shown in Figure 1f). Here it is noticeable that if there is no PVP participation, as shown in Figure S1a, CdS nanoparticles and MoS_2/G nanosheets are separate. In addition, as shown in Figure S1b, the MoS_2 sheets and CdS particles are also separate, indicating the smaller surface area and lower content of vacancies for pure MoS_2. From Figure 1g to j, it can be seen that CdS nanoparticles are uniformly and compactly grown on the surface of MoS_2/G nanosheets. Additionally, the crystallinity of MoS_2/G composites is improved after the annealing process. HRTEM images in Figure 1i and j show a typical layered MoS_2 with an interlayer distance of 0.62 nm, which is in accordance with the information on the (002) peak of MoS_2. According to the Scherrer equation ($D = K\lambda/\beta \cos\theta$), the average *c*-stacking height, calculated from the (002) reflection, is 4–5 nm for MoS_2/G, and the average number of layers is reasonably estimated to be 6 or 7. It has been reported that the thinner MoS_2 sheets show higher electron mobility than that of bulk MoS_2, especially the single-layer MoS_2 sheets, which show ultrahigh electron mobility, similar to that of graphene nanoribbons.[35] In our proposed MoS_2/G nanosheets, few-layered MoS_2 composited with graphene was supposed to show high electron mobility.

To understand the microstructure of precursors in the composite, the TEM and XRD analyses of MoS_2, MoS_2/G, and CdS are shown in Figure 2. Compared to

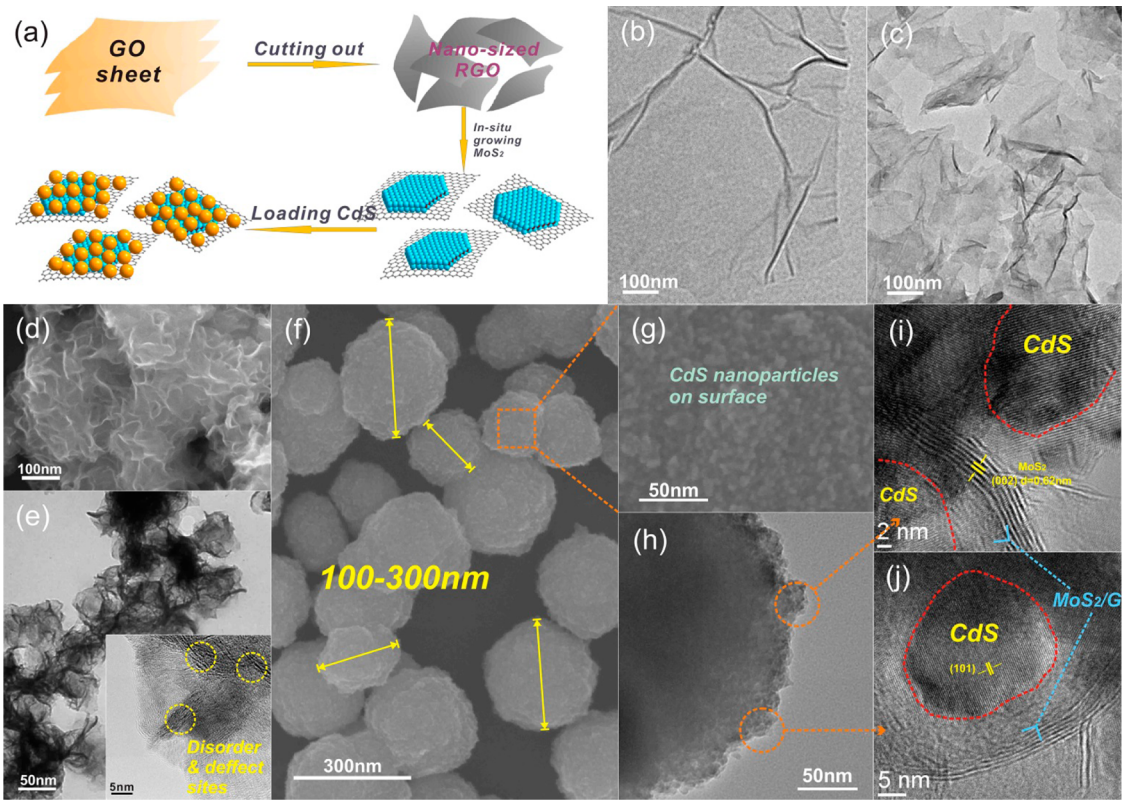

Figure 1. (a) Schematic illustration of growth mechanism of MoS_2/G-CdS composites; (b) TEM image of graphene oxide; (c) TEM image of nanosized reduced graphene oxide; (d) SEM image of as-prepared MoS_2/G composite; (e) TEM image of as-prepared MoS_2/G composites; the inset is the HRTEM image of as-prepared MoS_2/G composites; (f) SEM image of MoS_2/G-CdS composites after annealing at 573 K for 2 h in an Ar atmosphere, in which the molar ratio of MoS_2 to graphene is 1:2 and the amount of MoS_2/G is 2.0 wt %; (g) SEM image of partial enlargement of the surface of the MoS_2/G-CdS composite; (h) TEM image of the MoS_2/G-CdS composite; (i and j) HRTEM images of the MoS_2/G-CdS composite.

the MoS_2/G, pure MoS_2 has a higher crystallization degree and thicker sheets, indicating that due to the large surface of graphene, MoS_2 nanoparticles are better dispersed on the graphene. In addition, the as-prepared MoS_2/G nanosheets with a thickness of ~4 nm are thinner than that of pure MoS_2 (~14 nm), indicating that graphene sheets greatly inhibit the restacking of MoS_2 layers.[36] Furthermore, according to the Brunauer–Emmett–Teller (BET) adsorption–desorption isotherms in Figure S2, it can be calculated that the surface area of as-prepared MoS_2/G is 63.2 m^2/g, which is larger than that of pure MoS_2 (24.2 m^2/g). It is indicated that the introduction of graphene increased the specific surface area of the composites. As shown in Figure 2c, while the as-prepared MoS_2 shows a low crystallinity and amorphous structure, MoS_2 and MoS_2/G synthesized by L-cysteine exhibit high crystallinity and a typical hexagonal structure after annealing in Ar at 573 K, which is in accordance with those established by JCPDS card number 37-1492. Here it is worth noticing that the (002) diffraction peak of the graphene nanosheets cannot be detected, indicating that the graphene nanosheets do not stack during the hydrothermal process and annealing. Free CdS nanoparticles are shown in Figure 2d, and it can be seen that the free CdS by this proposed method delivers a small particle size of ~10 nm and good crystallinity, which is beneficial to photoelectrons transiting to the surface, improving the reaction activities.

To understand the role of MoS_2/G in MoS_2/G-CdS composites, the surface area and porosity of free CdS and MoS_2/G-CdS composites have been investigated, as displayed in Figure 3. It can be seen that the introduction of few-layer MoS_2/G has an effect on the pore structure of the samples. The BET surface areas of free CdS and MoS_2/G-CdS composites are measured to be 91.6 and 89.8 m^2/g, respectively. While both samples have similar surface areas, the pore size distributions (inset) are different. It is obviously seen that for free CdS the pore is produced by the accumulation of nanoparticles and the size is from 1 to 20 nm. But for MoS_2/G-CdS composites, most of the pores are less than 5 nm, which is because of the tight adsorption of Cd^{2+} ions on the defect sites and vacancies of the MoS_2/G matrix. Under the adhesive effect of PVP, 3D hierarchical MoS_2/G-CdS composites are obtained. This kind of porous 3D hierarchical structure was supposed to be beneficial for solution infiltration and photogenerated electron mobility, improving the photocatalytic H_2 evolution activities.

Figure 4 shows the UV–vis diffuse reflectance spectra of CdS, graphene/CdS, MoS_2/CdS, and MoS_2/G-CdS samples. It can be seen that pure CdS can absorb visible

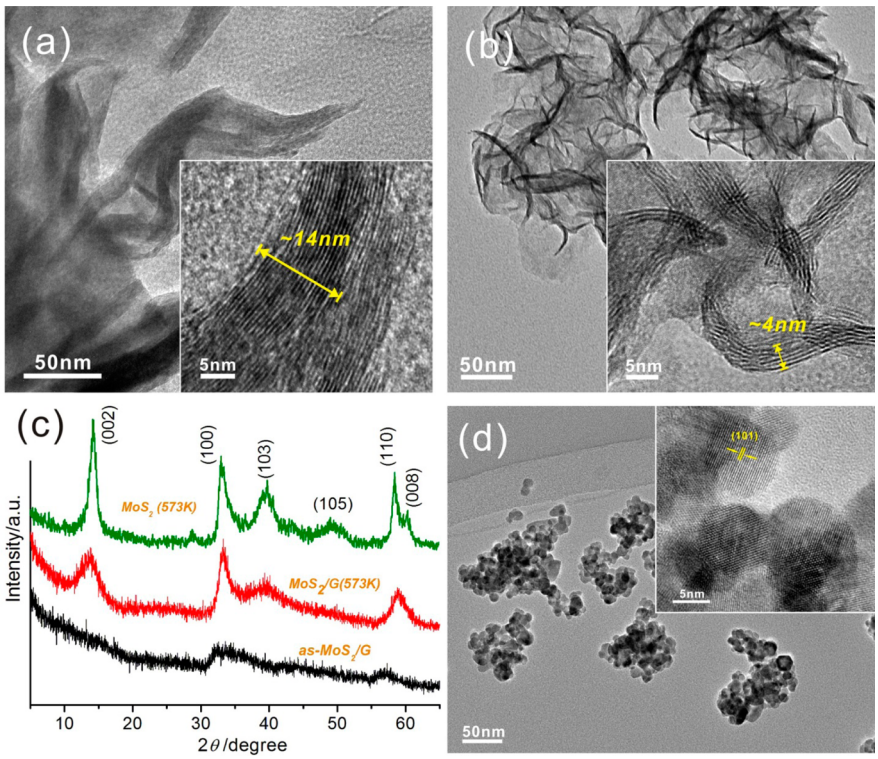

Figure 2. (a) TEM image of pure MoS_2 after annealing at 573 K for 2 h in an Ar atmosphere; the inset is its HRTEM image; (b) TEM image of the MoS_2/G composite after annealing at 573 K for 2 h in an Ar atmosphere in which the molar ratio of MoS_2 to graphene is 1:2; (c) XRD patterns of as-prepared MoS_2/G, MoS_2/G, and MoS_2 after annealing at 573 K for 2 h in an Ar atmosphere; (d) TEM image of pure CdS nanoparticles after annealing at 573 K for 2 h in an Ar atmosphere; the inset is its HRTEM image.

light with wavelengths of about 520 nm for its corresponding band gap of 2.4 eV. Adding MoS_2, graphene, or MoS_2/G cocatalysts will all increase their absorption under UV and visible light. This is because of their narrow band gap and deep color, which is beneficial for the photocatalytic activity. The band gaps of synthesized MoS_2 and MoS_2/G cocatalysts were measured by UV−vis spectra (Figure S3a and b). It can be seen that the synthesized MoS_2 and MoS_2/G exhibit a narrow band gap (indirect, ~1.0 eV), which is narrower than the values reported in the literature (1.1−1.3 eV). This might be caused by the lower crystallinity and defects in the synthesized MoS_2. Generally, the increase of defect degree will lead to narrowing of the band gap.[37,38]

Optimizing of Components in MoS_2/G-CdS for HER. The photocatalytic hydrogen production activities of the aforementioned samples are measured and compared in Figure 5. Figure 5a shows the rate of H_2 evolution of samples with different weight amounts of MoS_2/G cocatalysts. It can be seen that pure MoS_2/G composites do not show any photocatalytic H_2 evolution activities and thereby can be used only as cocatalysts. Pure CdS shows negligible activities because of recombination of electron−hole pairs. However, the MoS_2/G-CdS composites exhibit obvious photocatalytic hydrogen production activities due to the recombination delay of electron−hole pairs by MoS_2/G. Especially, the composite with 2.0 wt % content of MoS_2/G cocatalyst shows the highest hydrogen production rate of 1220.6 μmol/h and 5931.5 μmol after 5 h irradiation, corresponding to an apparent quantum efficiency (AQE) of 20.6% at 420 nm. The H_2 evolution rate will be decreased with an increase in content of MoS_2/G cocatalyst, which because of too much black MoS_2/G composites would block the transition of photons. Generally, the cocatalytic activities of MoS_2 are caused by the active S atoms on its exposed edges, but the S atoms on the basal plane have no activity, which hinders full utilization of MoS_2 as a cocatalyst. Therefore, the introduction of graphene can solve this problem to a certain extent due to its high conductivity. Obviously, as shown in Figure 5b, the cocatalytic activity of MoS_2/G is far higher than pure MoS_2. Previous studies indicated that graphene could improve the transfer of the photogenerated electrons in the conduction band of catalysts to the edges of MoS_2 and then react with adsorbed H^+ ions to form H_2.[31] In addition, the high concentration of electrons between the MoS_2 layer and the graphene layer could greatly enhance the electronic conductivity of composites,[39] and therefore the cocatalytic activities of composites are improved significantly.

In our previous work, we demonstrated that MoS_2 could uniformly disperse on the graphene when the molar ratio of MoS_2 to graphene is 1:2, and this kind of composite exhibited the most enhanced synergetic effect between MoS_2 and graphene, facilitating the

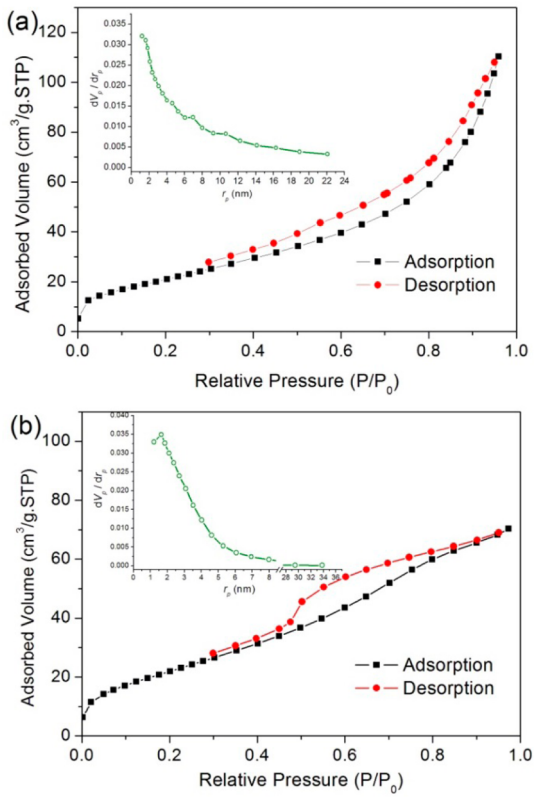

Figure 3. BET adsorption−desorption isotherms of (a) free CdS nanoparticles and (b) MoS_2/G-CdS composites after annealing at 573 K for 2 h in an Ar atmosphere, in which the molar ratio of MoS_2 to graphene is 1:2 and the amount of MoS_2/G is 2.0 wt %; inset is the corresponding pore size distribution by the BJH method.

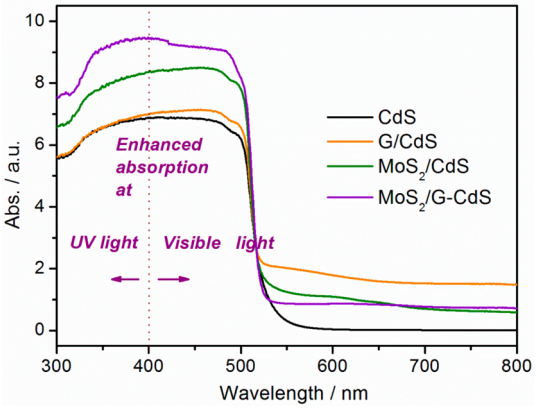

Figure 4. UV−vis spectra of CdS, graphene/CdS, MoS_2/CdS, and MoS_2/G-CdS samples that were annealed at 573 K for 2 h in an Ar atmosphere. The cocatalyst amount is 2.0 wt %.

charge transition.[34,39−41] Here, for different contents of MoS_2/G cocatalysts, the MoS_2/G with a molar ratio of 1:2 of MoS_2:G exhibited the highest cocatalytic activity for photocatalytic H_2 evolution. From Figure 5b, it can be seen that CdS/graphene (without MoS_2) shows very low photocatalytic H_2 evolution activities (only 167.5 μmol/h), but still higher than that of pure CdS (62.3 μmol/h), indicating that graphene also has some cocatalytic activity on H_2 evolution because of its more negative redox potential than H^+/H_2 (Figure S3c). However, due to the lesser H^+ adsorption ability of C atoms than active S atoms, the cocatalytic activity of graphene is much less than that of MoS_2. Furthermore, the stability of the photocatalysts also depended on their degree of crystallization.

Figure 5c and d show the photocatalytic H_2 production activities of MoS_2/G-CdS with 2.0 wt % cocatalyst and a molar ratio of MoS_2 to graphene of 1:2, annealing at different temperatures. It can be seen that when annealed at more than 573 K, photocatalysts exhibit a high H_2 evolution activity and stable cycling behavior. Especially when the annealing temperature is 573 K, the MoS_2/G-CdS composite delivers the highest H_2 evolution activity, which can be explained in Figure 6. At the lower annealing temperature, the degree of crystallization is low, which is not advantageous to photogenerated electrons migrating to the surface for reactions, but at a too high temperature (673 K), the CdS particles are easily agglomerated and grow to large particles, and besides, the MoS_2/G cocatalysts could not uniformly disperse on the surface of CdS (as shown in Figure S4), not facilitating the charge transition. Therefore, MoS_2/G-CdS composites can exhibit the best photocatalytic H_2 evolution activities at an annealing temperature of 573 K. It is well known that Pt is a very high efficiency cocatalyst for traditional photocatalysts in H_2 evolution reactions, and the commen loading method is photodeposition. In our experiment, we found that 0.5 wt % of Pt loading on CdS exhibited the highest photocatalytic activity toward H_2 evolution. As shown in Figure 5e, the rate of 3.3 mmol/h H_2 generation is much higher than that of the MoS_2/G-CdS composite (1.2 mmol) in $Na_2S−Na_2SO_3$ solution, although the process of loading Pt by photodeposition needed 2 h (as shown in Figure 5f). It is indicated that the MoS_2/G-CdS composite still has a large gap with Pt/CdS in H_2 evolution in $Na_2S−Na_2SO_3$ solution. However, due to the escaping of H_2S in Na_2S solution, which could be environmentally hazardous, the $Na_2S−Na_2SO_3$ system as the sacrificial agent necessitates the determination of an alternative environmentally friendly sacrificial agent.

H_2 Evolution Activity in Lactic Acid Solution. Figure 7 shows the photocatalytic H_2 production activities of CdS, MoS_2/CdS, MoS_2/G-CdS, graphene/CdS, and Pt/CdS (0.5 wt %) in lactic acid solution. It can be seen that the photocatalytic activity of pure CdS and graphene/CdS in lactic acid solution is still negligible because of recombination of electron−hole pairs, and graphene could not effectively separate the electron−hole pairs. In addition, as shown in Figure S5, it is found that the oxidation potential of CdS in $Na_2S−Na_2SO_3$ solution is lower than the case in lactic acid solution, indicating the easier oxidation of CdS in $Na_2S−Na_2SO_3$ solution. However, after loading MoS_2 cocatalyst, the MoS_2/CdS composite exhibits a largely enhanced photocatalytic activity for HER with about 1.13 mmol

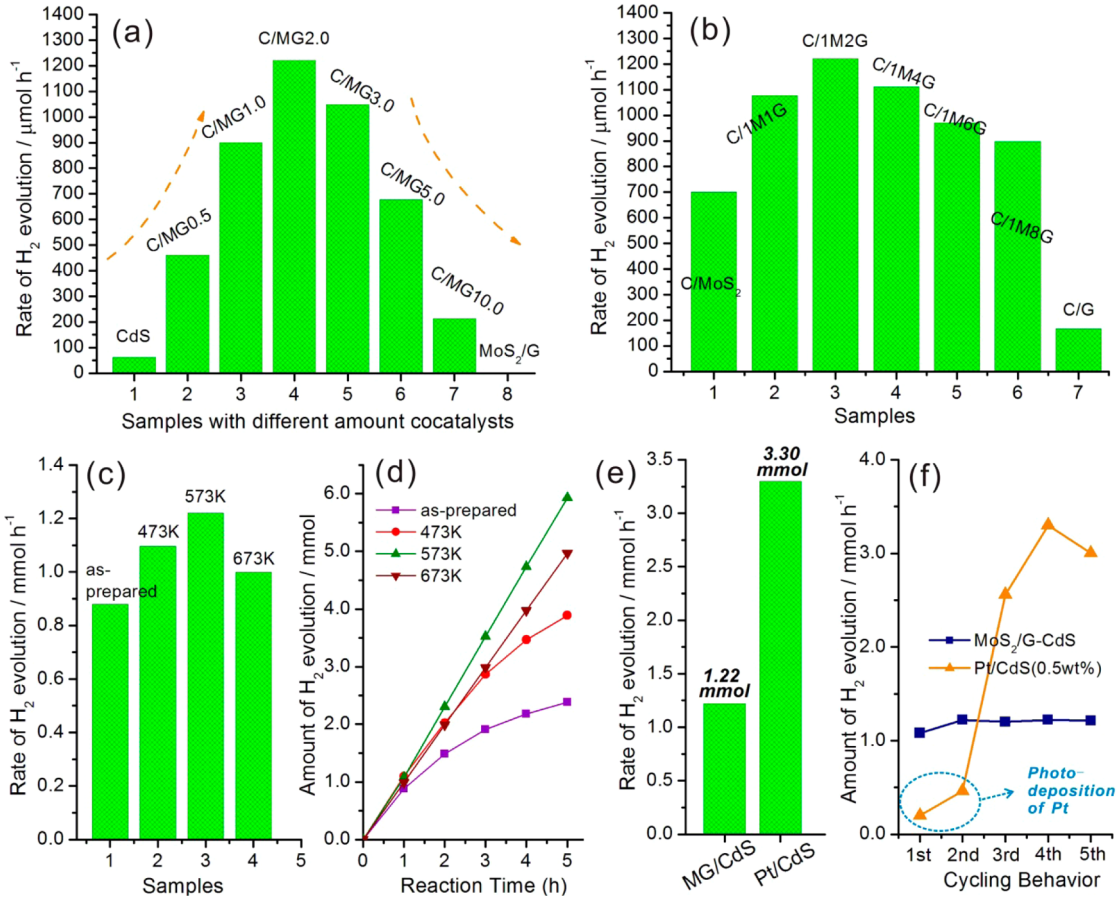

Figure 5. Photocatalytic H_2 evolution of MoS_2/G-CdS composites and Pt/CdS. (a) Comparison of photocatalytic H_2 production activities of different samples with different weight amounts of cocatalysts for 1 h; (b) photocatalytic H_2 production activities of different samples with different molar contents of MoS_2/G in which the amount of cocatalyst is 2.0 wt %; (c) photocatalytic H_2 production activities of MoS_2/G-CdS with 2.0 wt % cocatalyst and a molar ratio of MoS_2 to graphene of 1:2, annealing at different temperatures, and (d) their cycling behavior in 5 h; (e) photocatalytic H_2 production activities of the MoS_2/G-CdS composite and Pt/CdS (0.5 wt %) with the highest H_2 generation for 1 h and (f) their cycling behavior at 5 h. Light source: 300 W Xe lamp, λ > 420 nm. Reaction solution: 300 mL of 0.35 mol/L of Na_2S−Na_2SO_3 aqueous solution. Cat. 0.2 g.

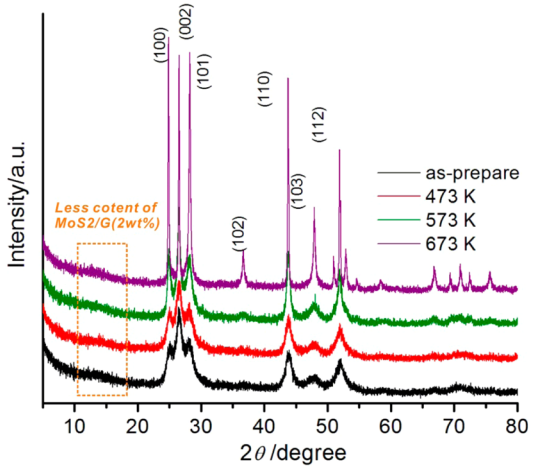

Figure 6. XRD patterns of MoS_2/G-CdS with 2.0 wt % cocatalyst and a molar ratio of MoS_2 to graphene of 1:2, annealing at different temperatures for 2 h in an Ar atmosphere.

in the first hour and 6.3 mmol after 5 h of irradiation (as shown in Figure 7a and b). Furthermore, the optimized MoS_2/G-CdS composite shows the highest photocatalytic activity for HER with about 1.6 mmol in the first hour and 9 mmol after 5 h of irradiation, which is not only higher than that of Pt/CdS (~0.276 mmol/h) but also higher than its case in Na_2S−Na_2SO_3 solution. Figure 7c shows the cycling behavior of the amount of hydrogen generation of different samples per hour. It can be seen that the average hydrogen generation rate of MoS_2/G-CdS is about 1.8 mmol/h, corresponding to an apparent quantum efficiency of 28.1% at 420 nm, which is higher than that of the MoS_2/CdS composite (the average hydrogen generation rate is about 1.28 mmol/h), indicating that the incorporation of graphene considerably enhances the photocatalytic activities of the composite. However, for Pt/CdS, the hydrogen generation rate decreases with time. This might be caused by a poisoning phenomenon of Pt by the −CO group from the degradation of lactic acid, which is usually seen in the field of fuel cells.[42,43]

Mechanism of Photocatalysis for HER. As in many reports, the active S atoms on exposed edges of MoS_2 increase

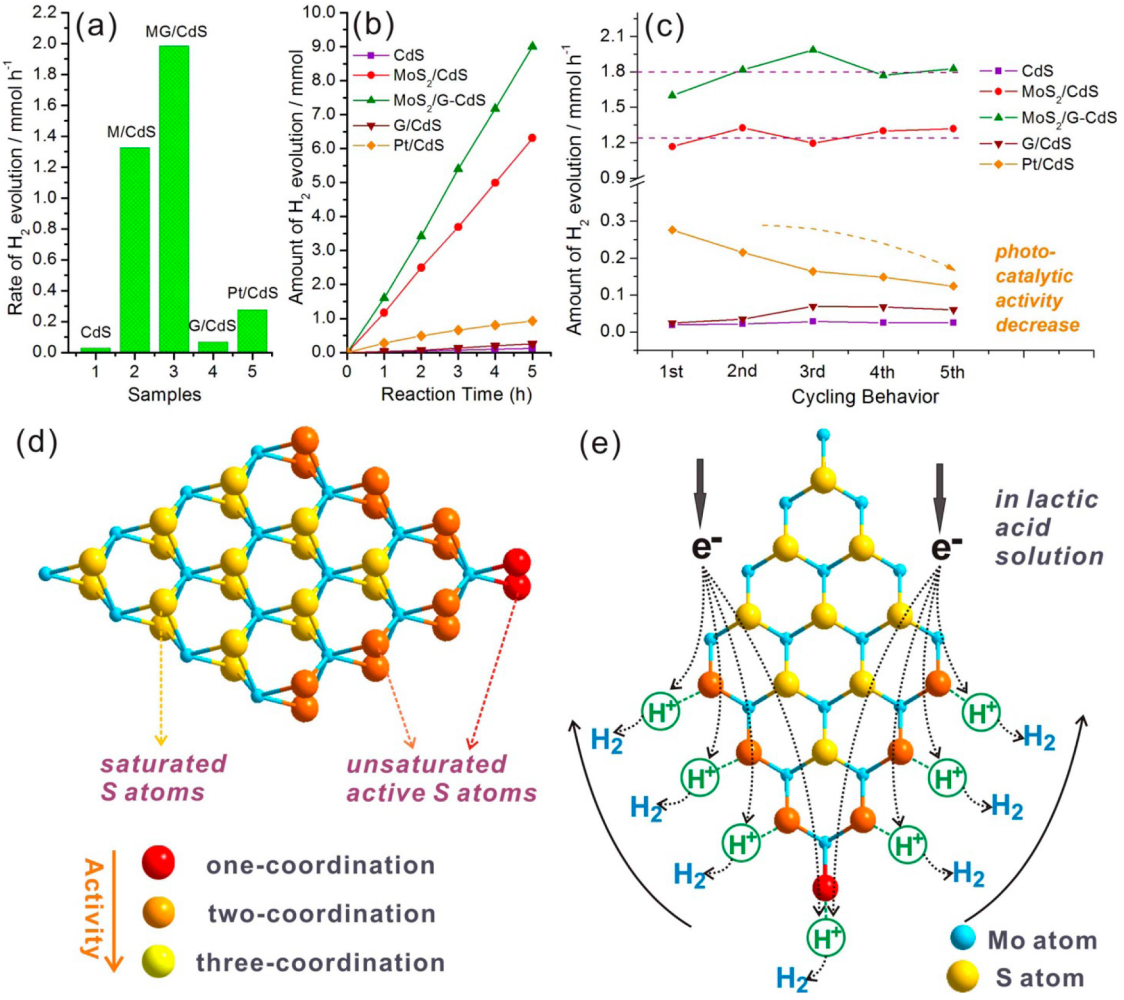

Figure 7. (a) Photocatalytic H_2 production activities of CdS, MoS_2/CdS, optimized MoS_2/G-CdS, graphene/CdS, and Pt/CdS (0.5 wt %) with the highest H_2 generation for 1 h and (b) their amount of H_2 generation in 5 h; (c) photocatalytic cycling behavior of samples per hour. Light source: 300 W Xe lamp, $\lambda > 420$ nm. Reaction solution: 300 mL of lactic acid aqueous solution (20%). Cat. 0.2 g. (d) Schematic illustration of the microstructure of MoS_2 and (e) its cocatalytic mechanism of H_2 generation in lactic acid solution.

its activity for HER.[21,22] Yan *et al.* demonstrated that the unsaturated active S atoms in MoS_2 could improve the electrocatalytic properties of MoS_2.[44] Given this, a schematic illustration of the microstructure of MoS_2 and its cocatalytic mechanism of H_2 generation are shown in Figure 7d and e. It can be seen that the activities of S atoms in the MoS_2 molecule are different with respect to their different coordination. The S atoms marked by red color with monocoordination have the highest activity, which is higher than that marked by orange color with two-coordination. Both kinds of S atoms are unsaturated active S atoms that have strong bonds to H^+ in the solution, which are easily reduced to H_2 by electrons. Due to the abundance of H^+ ions in the lactic acid solution, the unsaturated active S atoms on exposed edges of MoS_2 more easily capture H^+ ions than is the case in $Na_2S-Na_2SO_3$ solution, facilitating H_2 generation. Nevertheless, the S atoms on the basal plane with three-coordination are saturated atoms that have no activity. Thereby, nanoscale MoS_2 is highly active for H_2 evolution as a result of the quantum-confinement effect. In this paper, the nanosized few-layer MoS_2 has more exposed edges and unsaturated active S atoms and exhibits a good cocatalytic activity for HER.

As mentioned before, the poor electrical conductivity of pure MoS_2 restricts its cocatalytic activity in HER. As a good two-dimensional layered conductor, graphene could greatly match with layered MoS_2 and enhance its conductivity, facilitating fast charge transfer. A tentative mechanism proposed for the high H_2 production activity of the MoS_2/G-CdS composite is illustrated in Figure 8a. Under visible light, the photogenerated electrons of CdS are excited and transferred to the surface. Some of the electrons approaching the edge of MoS_2 are directly reacted with adsorbed H^+ in H_2O to produce H_2 under the cocatalytic activities of unsaturated active S atoms, which can accept electrons and act as active sites for H_2 generation.[45] Other electrons on the MoS_2/G basal planes, which have no catalytic activity, can be transferred to the edge of MoS_2 through the graphene sheets and then react with

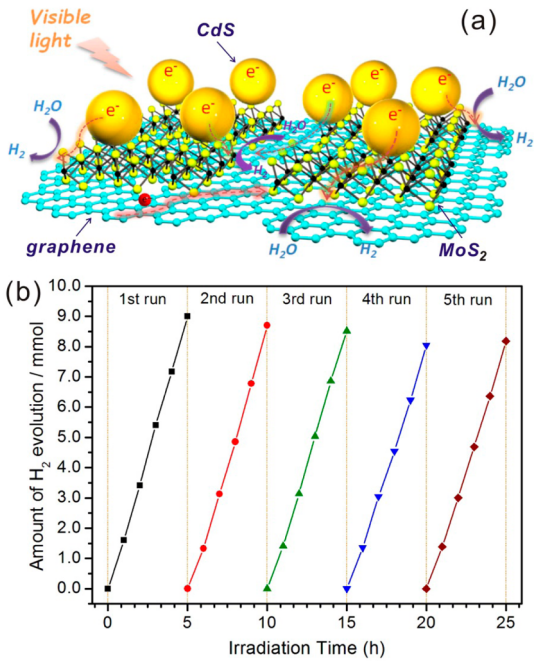

Figure 8. (a) Schematic illustration of the charge transfer in the MoS_2/G-CdS composite under visible light irradiation. Graphene provides a template for photogenerated electron transfer. (b) Cycling test of photocatalytic H_2 evolution for MoS_2/G-CdS composites with 2.0 wt % cocatalyst and a molar ratio of MoS_2 to graphene of 1:2, annealing at 573 K for 2 h. Light source: 300 W Xe lamp, $\lambda > 420$ nm. Reaction solution: 300 mL of a lactic acid aqueous solution (20%). Cat. 0.2 g.

adsorbed H^+ at the edges of MoS_2 to form H_2. Previous studies have shown that the layer numbers of MoS_2 deliver the different H_2 evolution potential, and fewer layers lead to a more negative potential, facilitating the water splitting.[31,46] In the proposed MoS_2/G composites, due to the inhibition of the (002) plane of MoS_2 along the *c*-axis by graphene sheets, the obtained few-layer MoS_2/G composites show high cocatalytic photocatalytic H_2 evolution activities for CdS. In addition, the nanosized MoS_2/G sheets have more active edges, which shorten the path of electron transfer. This possible mechanism can be further confirmed by transient photocurrent experiments (Figure S6). Pure CdS shows a very low photocurrent density because of the rapid recombination of the photogenerated electrons and holes. After adding MoS_2 or graphene cocatalysts, the photocurrent densities are significantly enhanced, indicating that the recombination of electron–hole pairs is delayed. The MoS_2/G-CdS composite shows the highest photocurrent density, indicating the improved charge transportation from CdS to the edge of MoS_2 through graphene. Additionally, from Figure S7 it can be seen clearly that the introduction of graphene indeed enhanced the electrical conductivity of the composite. Futhermore, the stability of MoS_2/G-CdS (2 wt %, Mo:G = 1:2) was tested by using the same catalyst for photocatalytic H_2 production repeatedly five times (as shown in Figure 8b). After five recycles, the catalyst did not show significant loss of activity, indicating its high stability during photocatalytic H_2 evolution. It is believed that a semiconductor with a small particle size and high crystallinity will show good photocatalytic activity and stability. In this article, for the nanosized CdS particle, due to its short distance between the core and its surface, the photogenerated electrons and holes could be easy transferred to the surface for reaction, effectively improving the photoelectric transformation efficiency and stability. Therefore, this kind of MoS_2/G-CdS composite would find wide applications as a promising photocatalyst with high efficiency and low cost for the photocatalytic H_2 evolution reaction.

CONCLUSIONS

A facile process was developed to synthesize CdS-based composite photocatalysts containing a few-layered MoS_2/G cocatalyst. The characterizations demonstrate that the layered MoS_2 molecules are tightly supported on the graphene surface and CdS nanoparticles were uniformly loaded on the MoS_2/G composite. Through the optimizing of each component proportion, the MoS_2/G-CdS composite showed the highest photocatalytic H_2 production activity when the content of the MoS_2/graphene cocatalyst is 2.0 wt % and the molar ratio of MoS_2 to graphene is 1:2. The photocatalytic H_2 evolution activity of the proposed MoS_2/G-CdS composite was tested and compared in Na_2S–Na_2SO_3 solution and lactic acid solution. A 1.8 mmol/h H_2 evolution rate in lactic acid solution corresponding to an AQE of 28.1% at 420 nm is not only higher than the case in Na_2S–Na_2SO_3 solution of 1.2 mmol/h, corresponding to an AQE of 20.6%, but also much higher than that of Pt/CdS in lactic acid solution. It is demonstrated that due to the high activity of adsorbed H^+ ions of unsaturated active S atoms on exposed edge of MoS_2, the photogenerated electrons could directly or through the graphene substrate react with H^+ ions to form H_2. It is believed that the incorporation of graphene enhances the charge transfer abilities and retards the recombination of electron–hole pairs, improving the photocatalytic H_2 evolution activities. Therefore, this kind of noble-metal-free MoS_2/G-CdS composite has great potential for photocatalytic H_2 production under visible light irradiation.

EXPERIMENTAL METHODS

Synthesis of Graphene Oxide and Nanosized RGO. Natural flake graphite (Aldrich, +100 mesh) was oxidized to graphite oxide using a modified Hummers method.[47] Typically, graphite powder (1.0 g) and sodium nitrate (0.75 g) were first stirred in concentrated sulfuric acid (37.5 mL) while being cooled in an ice–water bath. Then potassium permanganate (4.5 g) was gradually added to form a new mixture. After 2 h in an

ice–water bath, the mixture was allowed to stand for 5 days at room temperature with gentle stirring. Then, 100 mL of a 5 wt % H_2SO_4 aqueous solution was added into the above mixture over 1 h with stirring. Then, 3 g of H_2O_2 (30 wt % aqueous solution) was also added to the above liquid, and the mixture was stirred for 2 h. After that, the suspension was washed until the pH value of the filtrate was neutral. The obtained solid GO was dispersed in water and sonicated (40 kHz, 500 W) for 30 min under ambient conditions until the solution became clear. Then dispersion was then centrifuged at 2000 rpm for 15 min to remove any unexfoliated GO. The GO solution was quantified as 1.2 mg/mL. The nanosized RGO was prepared by hydrothermal reaction of as-prepared GO solution and NaOH. NaOH (20 mg) was added to 60 mL of GO solution and sonicated for 2 h to obtain a uniform solution. Then 0.5 mL of hydrazine hydrate was added into the above mixture. The hydrothermal reduction was carried out in a 100 mL autoclave at 373 K for 12 h.

Synthesis of MoS_2, MoS_2/Graphene, CdS, CdS/Graphene, and MoS_2/Graphene-CdS. A mixture of 0.5 g of Na_2MoO_4 and 0.8 g of L-cysteine was dissolved in 80 mL of DI water and then transferred into a 100 mL Teflon-lined stainless steel autoclave, sealed tightly, and heated at 453 K for 24 h. After cooling naturally, the black precipitates were collected by centrifugation, washed with DI water and ethanol, and dried in a vacuum oven at 353 K overnight. With the same method as above, adding different amounts of RGO (according to the molar ratios of Mo:C of 1:1, 1:2, 1:4, 1:6, and 1:8, corresponding to a weight ratio of RGO in composite of 7%, 13%, 23%, 31%, and 37%, respectively) into the starting materials solution, the as-prepared MoS_2/graphene powder could be obtained after washing and drying at 353 K overnight. To prepare the MoS_2/graphene-CdS composite, $CdCl_2$ and as-prepared MoS_2/graphene were dispersed in 300 mL of water with 10 g of polyvinylpyrrolidone, and Ar was bubbled throughout the solution to remove O_2. Then thioglycolic acid and 1.0 M NaOH were added into the solution as stabilizer and pH adjuster. After stirring for 2 h, 0.05 M $Na_2S \cdot 9H_2O$ was added at the rate of 0.05 mL/min and continuously stirred for 2 days. Finally, the products were washed by distilled water and ethanol several times. The obtained MoS_2/graphene-CdS composite was annealed at 473, 573, and 673 K for 2 h in an Ar atmosphere, respectively. As a control, CdS/graphene and free CdS were also synthesized by a solution-chemistry method under the same reaction conditions with and without adding RGO, at an annealing temperature of 573 K.

Characterizations. The samples were characterized by X-ray diffraction (RINT-2000; Rigaku Corp., Japan) with Cu $K\alpha_1$ radiation, a field emission scanning electron microscope (Hitachi S-4800), and a transmission electron microscope (TECNAI G2 F30, Japan). The Brunauer–Emmett–Teller surface areas were measured *via* nitrogen physisorption (Gemini2360; Micromeretics Corp., USA). The diffuse reflectance spectra of the samples were recorded on a UV–visible spectrophotometer (UV-2500PC; Shimadzu Corp., Japan) with barium sulfate as the reference. Then the absorption spectra were obtained from the reflectance spectra by means of Kubelka–Munk transformations.

Photocatalytic H_2 Evolution. The photocatalytic H_2 evolution was carried out with 0.2 g of photocatalyst suspended in a 300 mL solution in a Pyrex glass reaction cell. The reaction cell was connected to a gas-closed system with a gas-circulated pump. Visible light ($\lambda > 420$ nm) was generated by a 300 W Xe lamp combined with a UV-cutoff filter (L42, Hoya Co., Japan). The evolved H_2 was analyzed using an online gas chromatograph (GC-8A, Shimadzu Co., Japan) equipped with a thermal conductivity detector. The apparent quantum efficiency was measured by applying a Xe lamp (300 W) with a 420 nm bandpass filter (MIF-W, Optical Coatings Japan Co., Japan). The number of incident photons was measured using a radiant power energy meter (Ushio spectroradiometer, USR-40). The AQE was calculated using the following equation:

$$\text{AQE}\ (\%) = \frac{\text{Number of reacted electrons}}{\text{Number of incident photons}} \times 100\%$$

$$= \frac{\text{Number of evolved } H_2 \text{ molecules} \times 2}{\text{Number of incident photons}} \times 100\%$$

Photoelectrochemical activity measurements were performed with a CHI electrochemical analyzer (ALS/CH model 650A) in a standard three-electrode system using the prepared samples as the working electrodes with an active area of *ca.* 2.0 cm^2, a Pt sheet as the counter electrode, and a Ag/AgCl (saturated KCl) electrode (RE-1C; BAS Inc.) as a reference electrode. The simulated sunlight was obtained by an AM 1.5 solar simulation (WXS-80C-3 AM 1.5G) with a light intensity of 100 mW/cm^2.

Conflict of Interest: The authors declare no competing financial interest.

Acknowledgment. This work was partially supported by the World Premier International Research Center Initiative (WPI Initiative) on Materials Nanoarchitectonics (MANA) and National Basic Research Program of China (973 Program, 2014CB239301).

Supporting Information Available: Supplementary figures and experimental data. This material is available free of charge *via* the Internet at http://pubs.acs.org.

REFERENCES AND NOTES

1. Hou, Y. D.; Abrams, B. L.; Vesborg, P. C. K.; Bjorketun, M. E.; Herbst, K.; Bech, L.; Setti, A. M.; Damsgaard, C. D.; Pedersen, T.; Hansen, O.; *et al*. Bioinspired Molecular Co-catalysts Bonded to a Silicon Photocathode for Solar Hydrogen Evolution. *Nat. Mater.* **2011**, *10*, 434–438.
2. Fujishima, A.; Honda, K. Electrochemical Photolysis of Water at a Semiconductor Electrode. *Nature* **1972**, *238*, 37–38.
3. Tong, H.; Ouyang, S. X.; Bi, Y. P.; Umezawa, N.; Oshikiri, M.; Ye, J. H. Nano-photocatalytic Materials: Possibilities and Challenges. *Adv. Mater.* **2012**, *24*, 229–251.
4. Ouyang, S. X.; Tong, H.; Umezawa, N.; Cao, J. Y.; Li, P.; Bi, Y. P.; Zhang, Y. J.; Ye, J. H. Surface-Alkalinization-Induced Enhancement of Photocatalytic H_2 Evolution over $SrTiO_3$-Based Photocatalysts. *J. Am. Chem. Soc.* **2012**, *134*, 1974–1977.
5. Yi, Z. G.; Ye, J. H.; Kikugawa, N.; Kako, T.; Ouyang, S. X.; Stuart-Williams, H.; Yang, H.; Cao, J. Y.; Luo, W. J.; Li, Z. S.; *et al*. An Orthophosphate Semiconductor with Photooxidation Properties under Visible-Light Irradiation. *Nat. Mater.* **2010**, *9*, 559–564.
6. Iwase, A.; Ng, Y. H.; Ishiguro, Y.; Kudo, A.; Amal, R. Reduced Graphene Oxide as a Solid-State Electron Mediator in Z-Scheme Photocatalytic Water Splitting under Visible Light. *J. Am. Chem. Soc.* **2011**, *133*, 11054–11057.
7. Kudo, A. Development of Photocatalyst Materials for Water Splitting. *Int. J. Hydrogen Energy* **2006**, *31*, 197–202.
8. Yan, H. J.; Yang, J. H.; Ma, G. J.; Wu, G. P.; Zong, X.; Lei, Z. B.; Shi, J. Y.; Li, C. Visible-Light-Driven Hydrogen Production with Extremely High Quantum Efficiency on Pt-PdS/CdS Photocatalyst. *J. Catal.* **2009**, *266*, 165–168.
9. Yang, S. B.; Gong, Y. J.; Zhang, J. S.; Zhan, L.; Ma, L. L.; Fang, Z. Y.; Vajtai, R.; Wang, X. C.; Ajayan, P. M. Exfoliated Graphitic Carbon Nitride Nanosheets as Efficient Catalysts for Hydrogen Evolution under Visible Light. *Adv. Mater.* **2013**, *25*, 2452–2456.
10. Yang, J. H.; Wang, D. G.; Han, H. X.; Li, C. Roles of Cocatalysts in Photocatalysis and Photoelectrocatalysis. *Acc. Chem. Res.* **2013**, *46*, 1900–1909.
11. Kudo, A.; Miseki, Y. Heterogeneous Photocatalyst Materials for Water Splitting. *Chem. Soc. Rev.* **2009**, *38*, 253–278.
12. Melian, E. P.; Lopez, C. R.; Mendez, A. O.; Diaz, O. G.; Suarez, M. N.; Rodriguez, J. M. D.; Navio, J. A.; Hevia, D. F. Hydrogen Production Using Pt-Loaded TiO_2 Photocatalysts. *Int. J. Hydrogen Energy* **2013**, *38*, 11737–11748.
13. Yang, J. H.; Yan, H. J.; Wang, X. L.; Wen, F. Y.; Wang, Z. J.; Fan, D. Y.; Shi, J. Y.; Li, C. Roles of Cocatalysts in Pt-PdS/CdS with Exceptionally High Quantum Efficiency for Photocatalytic Hydrogen Production. *J. Catal.* **2012**, *290*, 151–157.
14. Nguyen, M.; Tran, P. D.; Pramana, S. S.; Lee, R. L.; Batabyal, S. K.; Mathews, N.; Wong, L. H.; Graetzel, M. *In Situ* Photo-assisted Deposition of MoS_2 Electrocatalyst onto Zinc Cadmium Sulphide Nanoparticle Surfaces to Construct an Efficient Photocatalyst for Hydrogen Generation. *Nanoscale* **2013**, *5*, 1479–1482.

15. Zhang, J.; Yu, J. G.; Jaroniec, M.; Gong, J. R. Noble Metal-Free Reduced Graphene Oxide-$Zn_xCd_{1-x}S$ Nanocomposite with Enhanced Solar Photocatalytic H_2-Production Performance. *Nano Lett.* **2012**, *12*, 4584–4589.
16. Chen, G. P.; Li, D. M.; Li, F.; Fan, Y. Z.; Zhao, H. F.; Luo, Y. H.; Yu, R. C.; Meng, Q. B. Ball-Milling Combined Calcination Synthesis of MoS_2/CdS Photocatalysts for High Photocatalytic H_2 Evolution Activity under Visible Light Irradiation. *Appl. Catal., A* **2012**, *443*, 138–144.
17. Liu, Y.; Yu, Y. X.; Zhang, W. D. MoS_2/CdS Heterojunction with High Photoelectrochemical Activity for H_2 Evolution under Visible Light: The Role of MoS_2. *J. Phys. Chem. C* **2013**, *117*, 12949–12957.
18. Zhang, J.; Qiao, S. Z.; Qi, L. F.; Yu, J. G. Fabrication of NiS Modified CdS Nanorod p-n Junction Photocatalysts with Enhanced Visible-Light Photocatalytic H_2-Production Activity. *Phys. Chem. Chem. Phys.* **2013**, *15*, 12088–12094.
19. Li, Y. G.; Wang, H. L.; Xie, L. M.; Liang, Y. Y.; Hong, G. S.; Dai, H. J. MoS_2 Nanoparticles Grown on Graphene: An Advanced Catalyst for the Hydrogen Evolution Reaction. *J. Am. Chem. Soc.* **2011**, *133*, 7296–7299.
20. Jaramillo, T. F.; Jorgensen, K. P.; Bonde, J.; Nielsen, J. H.; Horch, S.; Chorkendorff, I. Identification of Active Edge Sites for Electrochemical H_2 Evolution from MoS_2 Nanocatalysts. *Science* **2007**, *317*, 100–102.
21. Karunadasa, H. I.; Montalvo, E.; Sun, Y. J.; Majda, M.; Long, J. R.; Chang, C. J. A Molecular MoS_2 Edge Site Mimic for Catalytic Hydrogen Generation. *Science* **2012**, *335*, 698–702.
22. Hinnemann, B.; Moses, P. G.; Bonde, J.; Jorgensen, K. P.; Nielsen, J. H.; Horch, S.; Chorkendorff, I.; Norskov, J. K. Biornimetic Hydrogen Evolution: MoS_2 Nanoparticles as Catalyst for Hydrogen Evolution. *J. Am. Chem. Soc.* **2005**, *127*, 5308–5309.
23. Kanda, S.; Akita, T.; Fujishima, M.; Tada, H. Facile Synthesis and Catalytic Activity of MoS_2/TiO_2 by a Photodeposition-Based Technique and its Oxidized Derivative MoO_3/TiO_2 with a Unique Photochromism. *J. Colloid Interface Sci.* **2011**, *354*, 607–610.
24. Zhou, W. J.; Yin, Z. Y.; Du, Y. P.; Huang, X.; Zeng, Z. Y.; Fan, Z. X.; Liu, H.; Wang, J. Y.; Zhang, H. Synthesis of Few-Layer MoS_2 Nanosheet-Coated TiO_2 Nanobelt Heterostructures for Enhanced Photocatalytic Activities. *Small* **2013**, *9*, 140–147.
25. Zong, X.; Yan, H. J.; Wu, G. P.; Ma, G. J.; Wen, F. Y.; Wang, L.; Li, C. Enhancement of Photocatalytic H_2 Evolution on CdS by Loading MoS_2 as Cocatalyst under Visible Light Irradiation. *J. Am. Chem. Soc.* **2008**, *130*, 7176–7177.
26. Lukowski, M. A.; Daniel, A. S.; Meng, F.; Forticaux, A.; Li, L. S.; Jin, S. Enhanced Hydrogen Evolution Catalysis from Chemically Exfoliated Metallic MoS_2 Nanosheets. *J. Am. Chem. Soc.* **2013**, *135*, 10274–10277.
27. Maitra, U.; Gupta, U.; De, M.; Datta, R.; Govindaraj, A.; Rao, C. N. R. Highly Effective Visible-Light-Induced H_2 Generation by Single-Layer 1T-MoS_2 and a Nanocomposite of Few-Layer 2H-MoS_2 with Heavily Nitrogenated Graphene. *Angew. Chem., Int. Ed.* **2013**, *52*, 13057–13061.
28. Jia, T. T.; Kolpin, A.; Ma, C. S.; Chan, R. C. T.; Kwok, W. M.; Tsang, S. C. E. A Graphene Dispersed CdS-MoS_2 Nanocrystal Ensemble for Cooperative Photocatalytic Hydrogen Production from Water. *Chem. Commun.* **2014**, *50*, 1185–1188.
29. Geim, A. K.; Novoselov, K. S. The Rise of Graphene. *Nat. Mater.* **2007**, *6*, 183–191.
30. Novoselov, K. S.; Morozov, S. V.; Mohinddin, T. M. G.; Ponomarenko, L. A.; Elias, D. C.; Yang, R.; Barbolina, I. I.; Blake, P.; Booth, T. J.; Jiang, D.; *et al*. Electronic Properties of Graphene. *Phys. Status Solidi B* **2007**, *244*, 4106–4111.
31. Xiang, Q. J.; Yu, J. G.; Jaroniec, M. Synergetic Effect of MoS_2 and Graphene as Cocatalysts for Enhanced Photocatalytic H_2 Production Activity of TiO_2 Nanoparticles. *J. Am. Chem. Soc.* **2012**, *134*, 6575–6578.
32. Pan, D. Y.; Zhang, J. C.; Li, Z.; Wu, M. H. Hydrothermal Route for Cutting Graphene Sheets into Blue-Luminescent Graphene Quantum Dots. *Adv. Mater.* **2010**, *22*, 734–738.
33. Ma, C.; Chen, Z. X.; Fang, M.; Lu, H. B. Controlled Synthesis of Graphene Sheets with Tunable Sizes by Hydrothermal Cutting. *J. Nanopart. Res.* **2012**, 14.
34. Chang, K.; Geng, D. S.; Li, X. F.; Yang, J. L.; Tang, Y. J.; Cai, M.; Li, R. Y.; Sun, X. L. Ultrathin MoS_2/Nitrogen-Doped Graphene Nanosheets with Highly Reversible Lithium Storage. *Adv. Energy Mater.* **2013**, *3*, 839–844.
35. Radisavljevic, B.; Radenovic, A.; Brivio, J.; Giacometti, V.; Kis, A. Single-Layer MoS_2 Transistors. *Nat. Nanotechnol.* **2011**, *6*, 147–150.
36. Chang, K.; Chen, W. X. L-Cysteine-Assisted Synthesis of Layered MoS_2/Graphene Composites with Excellent Electrochemical Performances for Lithium Ion Batteries. *ACS Nano* **2011**, *5*, 4720–4728.
37. Kam, K. K.; Parkinson, B. A. Detailed Photocurrent Spectroscopy of the Semiconducting Group-VI Transition-Metal Dichalcogenides. *J. Phys. Chem.* **1982**, *86*, 463–467.
38. Chen, X. B.; Liu, L.; Yu, P. Y.; Mao, S. S. Increasing Solar Absorption for Photocatalysis with Black Hydrogenated Titanium Dioxide Nanocrystals. *Science* **2011**, *331*, 746–750.
39. Chang, K.; Chen, W. X. *In Situ* Synthesis of MoS_2/Graphene Nanosheet Composites with Extraordinarily High Electrochemical Performance for Lithium Ion Batteries. *Chem. Commun.* **2011**, *47*, 4252–4254.
40. Chang, K.; Chen, W. X.; Ma, L.; Li, H.; Li, H.; Huang, F. H.; Xu, Z. D.; Zhang, Q. B.; Lee, J. Y. Graphene-like MoS_2/Amorphous Carbon Composites with High Capacity and Excellent Stability as Anode Materials for Lithium Ion Batteries. *J. Mater. Chem.* **2011**, *21*, 6251–6257.
41. Chang, K.; Chen, W. X. Single-Layer MoS_2/Graphene Dispersed in Amorphous Carbon: Towards High Electrochemical Performances in Rechargeable Lithium Ion Batteries. *J. Mater. Chem.* **2011**, *21*, 17175–17184.
42. Tiwari, J. N.; Tiwari, R. N.; Singh, G.; Kim, K. S. Recent Progress in the Development of Anode and Cathode Catalysts for Direct Methanol Fuel Cells. *Nano Energy* **2013**, *2*, 553–578.
43. Kang, Y. J.; Qi, L.; Li, M.; Diaz, R. E.; Su, D.; Adzic, R. R.; Stach, E.; Li, J.; Murray, C. B. Highly Active Pt_3Pb and Core-Shell Pt_3Pb-Pt Electrocatalysts for Formic Acid Oxidation. *ACS Nano* **2012**, *6*, 2818–2825.
44. Yan, Y.; Xia, B. Y.; Ge, X. M.; Liu, Z. L.; Wang, J. Y.; Wang, X. Ultrathin MoS_2 Nanoplates with Rich Active Sites as Highly Efficient Catalyst for Hydrogen Evolution. *ACS Appl. Mater. Interfaces* **2013**, *5*, 12794–12798.
45. Frame, F. A.; Osterloh, F. E. CdSe-MoS_2: A Quantum Size-Confined Photocatalyst for Hydrogen Evolution from Water under Visible Light. *J. Phys. Chem. C* **2010**, *114*, 10628–10633.
46. Linic, S.; Christopher, P.; Ingram, D. B. Plasmonic-Metal Nanostructures for Efficient Conversion of Solar to Chemical Energy. *Nat. Mater.* **2011**, *10*, 911–921.
47. Hummers, W. S.; Offeman, R. E. Preparation of Graphitic Oxide. *J. Am. Chem. Soc.* **1958**, *80*, 1339–1339.